Single-shot time-gated fluorescence lifetime imaging using three-frame images

Yahui Li[1,2,3], Hui Jia[3], Shaorong Chen[3,5], Jinshou Tian[1,2,6], Lingliang Liang[3], Fenfang Yuan[3], Hongqi Yu[3], David Day-Uei Li[4,7]

[1]Key Laboratory of Ultra-fast Photoelectric Diagnostics Technology, Xi'an Institute of Optics and Precision Mechanics, Xi'an, Shanxi 710049, China
[2]University of Chinese Academy of Sciences, Beijing 100049, China
[3]Laboratory of Ultra-fast Imaging, College of Electronic Science and Engineering, National University of Defense Technology, Changsha, Hunan 410073, China
[4]Faculty of Science, University of Strathclyde, Glasgow G4 0RE, Scotland, UK
[5] srchen@nudt.edu.cn
[6] tianjs@opt.ac.cn
[7]david.li@strath.ac.uk

Abstract

Qualitative and quantitative measurements of complex flows demand for fast single-shot fluorescence lifetime imaging (FLI) technology with high precision. A method, single-shot time-gated fluorescence lifetime imaging using three-frame images (TFI-TGFLI), is presented. To our knowledge, it is the first work to combine a three-gate rapid lifetime determination (RLD) scheme and a four-channel framing camera to achieve this goal. Different from previously proposed two-gate RLD schemes, TFI-TGFLI can provide a wider lifetime range 0.6 ~ 13ns with reasonable precision. The performances of the proposed approach have been examined by both Monte-Carlo simulations and toluene seeded gas mixing jet diagnosis experiments. The measured average lifetimes of the whole excited areas agree well with the results obtained by the streak camera, and they are 7.6ns (N_2 = 7L/min; O_2 < 0.1L/min) and 2.6ns (N_2 = 19L/min; O_2 = 1L/min) with the standard deviations of 1.7ns and 0.8ns among the lifetime image pixels, respectively. The concentration distributions of the quenchers and fluorescent species were further analyzed, and they are consistent with the

experimental settings.

1. Introduction

Planar laser-induced fluorescence (PLIF) sensing technologies are widely used in many scientific fields, such as airflow, combustion, and plasma diagnostics [1] due to its ability to measure the concentration, temperature, pressure and velocity [2, 3]. Compared to other diagnostic techniques such as coherent anti-Stokes Raman scattering (CARS) or tunable diode laser absorption spectroscopy (TDLAS), the advantage of PLIF is the ability to perform two-dimensional (2D) sliced wide-field imaging by shaping the excitation light into a light sheet [4]. Although the fluorescence signals carry the information about the concentrations of the probed species, it is challenging to conduct qualitative and quantitative measurements – multiple parameters need to be confirmed in order to either relatively compare or precisely obtain the species concentrations [5]. It is a challenging task to accurately assess the fluorescence quantum yield that is affected by collisions, simulated emissions, predissociations, and photoionizations. It is difficult to assess the impact of the collisional quenching in collisional processes, since the quenching depends on temperature, pressure, and quenchers, making PLIF only suitable for flow visualization. For example, OH-PLIF, CH_2O-PLIF, and CH-PLIF are used respectively to observe the reaction, preheating and heat releasing zones in a combustion field [6]. Accurately assessing the collisional quenching rate is the main key to achieving qualitative and quantitative measurements.

The collisional quenching rate can be directly determined by measuring the fluorescence lifetime. The fluorescence lifetime measurement techniques can be divided into time-domain and frequency-domain methods [7]. In time-domain methods [8], such as time-correlated single-photon counting (TCSPC) [9 ~ 11] and time-gated FLI [12 ~ 14], the fluorescence intensity decay is measured with pulsed laser excitations. In frequency-domain methods [15, 16], the sample is illuminated with a modulated light source. In addition, streak cameras can also be used to obtain time-resolved fluorescence intensity curves [17]. Unfortunately, these conventional FLI methods fail to observe instantaneous phenomena in a complex flow in 2D.

For non-repetitive dynamic events in complex flows and combustions, we expect to obtain the fluorescence lifetime images with a single excitation to freeze the instantaneous structures. Conventional time-gated FLI measures the fluorescence delay functions by gating the image intensifier of an ICCD camera with different delays. It usually needs to acquire more than one time-gated shot. Single-shot lifetime measurements can be achieved by replacing the single ICCD camera with two or more ICCD cameras to take time-resolved images simultaneously. Omrane *et al.* measured phosphorescence images with a high-speed framing camera containing eight independent ICCD image detectors, their system can obtain lifetimes in the order of milliseconds using an exponential fitting procedure [18]. However, this method is not suitable for measuring lifetimes around nanoseconds in a single shot. Ehn. *et al.* presented a single-shot FLI method with PLIF, using a dual ICCD detection setup with different gating characteristics for the two cameras, and they successfully demonstrated real-time acquisition of formaldehyde in a premixed, laminar methane/oxygen flame. The measured lifetimes range from 1.0 to 4.5ns [19].

The most traditional approach for lifetime estimations is to acquire a multipoint decay curve and analyze it with least-square methods. This approach, however, requires considerable acquisition and computational time and is therefore unsuitable for single-shot time-gated FLI. The rapid lifetime determination (RLD) method was previously proposed to allow analyzing the decay data in real-time. For single-exponential decays, the lifetimes can be easily evaluated. RLD is suitable for single-shot time-gated FLI, if two ICCD cameras are used. RLD has a variety of gating schemes [14, 20], such as the standard RLD (SRLD) using two gates of the same width or other more optimized RLD (ORLD) approaches. We can select a proper gating scheme to achieve a certain lifetime measurement range. In 2012, Ehn *et al.* achieved single-shot FLI of a toluene seeded gas mixture jet [21] using the same experimental setup as their earlier work [19], and they presented an evaluation algorithm, DIME (Dual Imaging and Modeling Evaluation), based on an ORLD scheme to evaluate image data. They estimated the lifetimes around 800ps with a standard deviation around 120ps (from 100 repeated measurements). Later they reported the fluorescence lifetime of toluene as a function

of the oxygen concentration in toluene/nitrogen/oxygen mixtures. The results agreed with the Stern-Volmer model, showing the potential for detecting the oxygen concentration through fluorescence lifetime measurements. Monte-Carlo simulations were performed to evaluate the sensitivity of DIME for oxygen detection. The results indicated a high measurement sensitivity in the range $0.5 \sim 6 mol/m^3$ [22], showing that DIME has potential for quantitative diagnosis of complex flows. However, traditional RLD methods have a drawback: they are unable to offer robust estimations if the samples to be tested have a wide range of lifetimes. In order to solve this problem, Ehn *et al.* also proposed an approach that the measurement precision is virtually insensitive to the lifetime with ramped gain functions for the two ICCD cameras. However, this solution requires extra modifications on the driving front-ends to generate the ramped gain function, which might be challenging to achieve.

We described an approach named 'single-shot time-gated fluorescence lifetime imaging using three-frame images (TFI-TGFLI)' to provide high-speed, high-precision and wide dynamic range ($0.6 \sim 13ns$) FLI. In this paper, we will firstly demonstrate the relationships between the fluorescence lifetimes and the quencher concentrations and the relationships between the pre-exponential factors and the fluorophore concentrations using the simple two-state fluorescence emission model. The TFI-TGFLI experimental setup will then be described. Secondly, we will introduce the lifetime (and pre-exponential factor) determination algorithm for TFI-TGFLI and will show the Monte-Carlo simulation results. Finally, the experimental results will be presented with the image data processed and analyzed to obtain the fluorescence lifetime images and the normalized fluorophore concentration images in two toluene-seeded gas mixing jets: 1) N_2 = 7L/min, O_2 < 0.1L/min (denoted as $N_2:O_2$ > 7:0.1 hereafter for simplicity), and 2) N_2 = 19L/min, O_2 = 1L/min (denoted as $N_2:O_2$ = 19:1 hereafter). The results will also be compared with those obtained from a streak camera.

2. Theory and experimental setup

Figure 1 shows a two-state system model of a fluorescent molecule [23]. The quantum states |1> and |2> are the ground state and the first excited state, respectively.

n_1 and n_2 are the concentrations at the states |1> and |2>. B_{12}, B_{21}, Q_{21} and A_{21} are the stimulated absorption, stimulated radiation, collisional quenching (non-radiation) and spontaneous emission probabilities, respectively. I_v is the intensity of the laser pulse in absorption lines. The rate equation at the state |2> can be expressed as

$$\dot{n}_2(t) = n_1(t)(I_v B_{12}) - n_2(t)(I_v B_{21} + Q_{21} + A_{21}) \ , \tag{1}$$

After the excitation, i.e. $I_v = 0$, $n_2(t) = n_2^{AE} \exp\left[-(Q_{21} + A_{21})t\right]$, where n_2^{AE} is the concentration at the state |2> after the excitation. Because the fluorescent signal is the spontaneous emission from the state |2>, the time resolved signal N_f can be derived as

$$N_f(t) = \frac{\Omega}{4\pi} \eta_c V A_{21} n_2(t) = A \exp(-t/\tau), \tag{2}$$

where,

$$A = \frac{\Omega}{4\pi} \eta_c V A_{21} n_2^{AE}, \tau = 1/(A_{21} + Q_{21}), \tag{3}$$

Ω is the solid angle for detection and V is the exited volume. η_c is the quantum efficiency of the collection optical system including a UV lens and a filter. Due to $A_{21} << Q_{21}$, $\tau \approx 1/Q_{21}$.

Under the weak excitation limit (linear LIF), $n_2 << n_1$, Eq. (1) can be transformed to $\dot{n}_2(t) = n_1^0(I_v B_{12})$, where n_1^0 is the concentration of the total toluene molecules at the states |1> before the laser excitation. Substituting $n_2^{AE} = \int n_1^0(I_v B_{12})dt$ for n_2^{AE} in Eq. (3), the pre-exponential factor A can be written as

$$A = \frac{\Omega}{4\pi} \eta_c V A_{21} B_{12} n_1^0 \int I_v dt. \tag{4}$$

Therefore, n_1^0 can be quantified by measuring A, which can be directly calculated from

$$S = \int A \exp(-t/\tau) dt, \tag{5}$$

with the lifetime τ being measured and A_{21}, B_{12}, and I_v already known. S is the integrated fluorescent intensity over the exposure time. We can conclude that measuring τ and A plays an important role in quantifying the concentrations of the quenchers and the fluorophores.
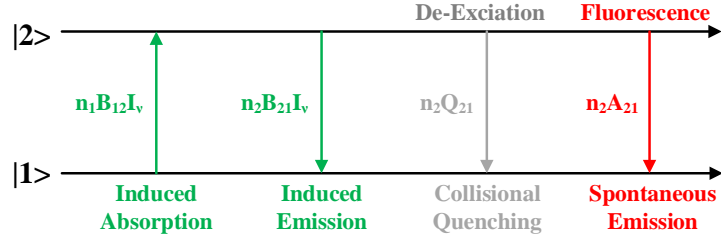
Fig. 1. Different transitions that are included in the two-state model.

The proposed TFI-TGFLI for estimating τ and A is to obtain three images in one single shot by a multi-channel framing camera, and then estimating τ and A images via the Newton–Raphson method. The experimental setup is shown in Fig. 2. A fourth harmonic pulsed Nd:YLF laser (the central wavelength = 263.25nm; the pulse duration = 10ps; the energy per pulse = 2mJ; the repetition rate = 5Hz; the beam diameter = 6mm) was used. A beam expander (including a negative lens and a positive lens) was used to expand the laser beam, and a cylindrical lens was used to focus the laser beam in one dimension (y axis as shown in Fig. 2). A laser sheet was formed around the focus point of the cylindrical lens. In our experiments, the output laser beam was directly focused by the cylindrical lens (f = 500mm) into a laser sheet aligned with the probe volume above a gas nozzle. The size of the laser sheet is 6mm×3mm (x×z). A 2mm-diameter jet tube (supplying toluene-seeded gas), was inserted at the center of a 5mm-diameter tube (providing a co-flow of gas shielding the central jet). The distance between the jet tube and the Nd:YLF laser is ~ 0.6m. The Nd:YLF laser sent a triggering pulse to the digital delay generator DG645 to trigger both the streak camera and the four-channel framing camera (XXRapidFrame, Stanford Computer Optics) to respectively record the filtered fluorescent signals with 300nm longpass filters. The distance between the jet tube and the lens of the framing camera is ~1m. The diagram of the multi-channel framing camera is also shown in Fig. 2. In the inset, a mirror image splitter behind an imaging lens splits an image into four sub images. The exposure time of each channel can be controlled by the image intensifier of the ICCD. The streak camera was used to record 1-D decay curves the compare with the results of TFI-TGFLI. The streak camera has a slit with 2mm width and 20mm length in parallel to the gas jet

(+x). And the measuring time window and scanning step are 40ns and 200ps, respectively. We used a UV lens (f = 60mm, F/1.7) to gather the signal to the streak camera. Additionally, the distance between the jet tube and the slit of the streak camera is ~0.3m. The directions of the laser propagation and the gas jet are in +z axis and +x axis, respectively.
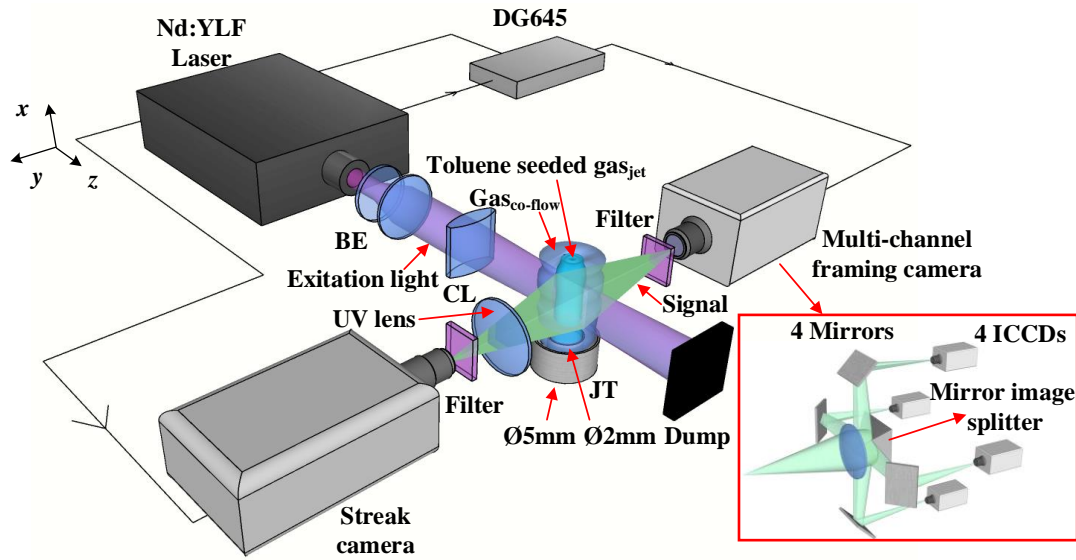

Fig. 2. Schematic illustration of the experimental setup. The laser beam is expanded through a beam expander (BE) and focused to a laser sheet by a cylindrical lens (CL) in the target area above the jet tubes (JT). A triggering pulse is sent to the digital delay generator DG645 to trigger both the streak camera and the framing camera to record filtered signals. The multi-channel framing camera contains an image splitter and four ICCDs.

3. The lifetime algorithm of TFI-TGFLI

This section describes the proposed three-gate rapid lifetime determination scheme, implemented on a newly developed four-channel framing camera to achieve single-shot FLI. We will compare its performance with an ORLD scheme [20].

The configuration of the three-gate RLD scheme is shown in Fig. 3, the black solid line is the normalized fluorescence intensity curve with a 10ps excitation pulse (red line). Since the fluorescence lifetime is usually a few nanoseconds, much greater than the pulsed laser duration 10ps, the fluorescent signals can be simplified as a single

exponential decay model, i.e. $N_f(t) = A\exp(-t/\tau)$. The effects of the IRFs are minor, and we can neglect the IRFs in our experiments. To examine this, we have conducted Monte-Carlo simulations. The results show that the lifetime estimations with our proposed algorithm are indeed insensitive to the IRF for single-exponential analysis. In fact, gating approaches are in general less sensitive (compared with traditional TCSPC approaches) to the imperfections of the IRF for single-exponential analysis. The impact of the IRF in our instruments contributed to errors only around 3% (for $\tau = 0.6$ns) and is therefore negligible in our discussions for simplicity. If the FWHM of the IRF is larger, we can time-shift the gate signal a bit away from the decay peak. This would sacrifice the photon efficiency a little bit, but for single-exponential analysis it is a well-known approach to reduce the bias [14, 24]. The orange, green, and purple areas represent three time-gates; their start times t^i_{start} and end times t^i_{end} (i = 1, 2, and 3) are listed in Table 1. TG represents 'time-gate'.
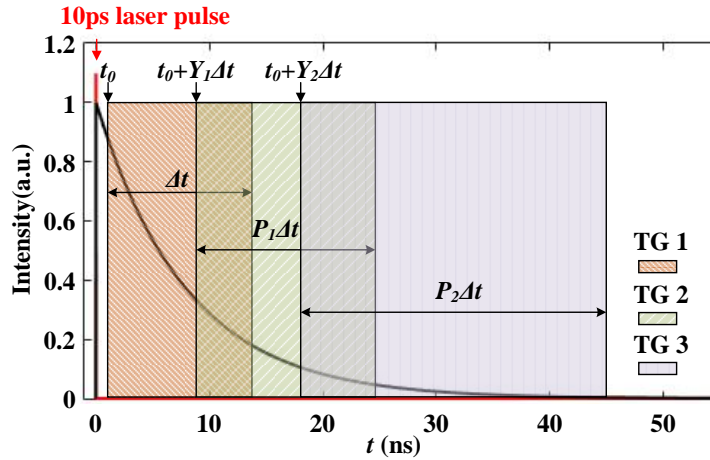

Fig. 3. Graphical illustration of the three time-gates used to estimate lifetimes.

Table 1. Time-gates configuration

TG i	TG 1	TG 2	TG 3
t^i_{start}	t_0	$t_0+Y_1\Delta t$	$t_0+Y_2\Delta t$
t^i_{end}	$t_0+\Delta t$	$t_0+(Y_1+P_1)\Delta t$	$t_0+(Y_2+P_2)\Delta t$

The time-gate parameters used in this article are $\Delta t = 3$ns, $Y_1 = 0$, $P_1 = 50/3$, $Y_2 = 1$, $P_2 = 50/3$. Two gating schemes can be formed with the three time-gates listed in

Table 2. Gating Scheme 1 consists of TGs 1 and 2; Gating Scheme 2 consists of TGs 2 and 3. The ranges in the parentheses represent the widths of the time-gates. The signal in TG i is

$$N_i = \int_{t_{start}^i}^{t_{end}^i} kp_i N_f dt, (i=1,2,3),\qquad(6)$$

k is the photoelectric conversion factor for the three channels, $k \sim \eta_{PC} G_{MCP} \eta_p C \eta_{CCD}$, where η_{PC} is the quantum efficiency of the photocathode, G_{MCP} is the gain factor of the microchannel plate, η_p is the quantum efficiency of the fluorescent screen, C is the coupling efficiency of the coupled optical system, and η_{CCD} is the quantum efficiency of the CCD, p_i is the percentage of the total signal. D_j is the ratio of the signal N_{j+1} to N_j, ($j=1,2$). For TFI-TGFLI, the coefficients k for the ICCD cameras in the framing camera are similar, therefore the effects caused by the differences in the gain functions (time-dependent gain) can be neglected.

Table 2. Two gating schemes

Gating Scheme 1		Gating Scheme 2	
TG 1 (0 ~ 3ns)	$D_1 = N_2/N_1$	TG 2 (0 ~ 50ns)	$D_2 = N_3/N_2$
TG 2 (0 ~ 50ns)		TG 3 (3 ~ 53ns)	

To achieve single-shot acquisition based on three-gate RLD, a four-channel framing camera can be used to split a signal into four channels equally to obtain three images in Channels 1, 2, and 3 with TGs 1, 2, and 3 respectively. The signal collected in each channel would decrease to $N_{tot}/4$, i.e. $p_i = 25\%$ ($i = 1, 2,$ and 3); N_{tot} is the total number of the photons detected by the framing camera. In this work, we present single-shot and wide dynamic-range FLI using three images ($i = 1, 2$ and 3), but we would also be able to fully use four images ($i = 1, 2, 3$ and 4) to improve the photon efficiency and to perform bi-exponential analysis in the future.

From D_1 and D_2, the lifetimes can be calculated rapidly and efficiently by using the Newton-Raphson method. We define

$$f_j(\tau) = \frac{N_{j+1}}{N_j} - D_j = 0, \ j = 1, \ 2.$$

The Newton iteration formula can be written as

$$\tau_{j,n+1} = \tau_{j,n} - f_j(\tau_{j,n})/f_j{'}(\tau_{j,n}), n = 0,1,2..., j = 1,2 \ , \tag{7}$$

where $\tau_{j,0}$ is initial value of the iteration, with $j = 1, 2$ representing Gating Schemes 1 and 2. Applying Eq. (7) to all pixels, and two lifetime images, τ_1 and τ_2, can be obtained. Hence, two A images (A_1 and A_2) can also be obtained by Eq. (5).

To simplify the discussions, the technical details regarding the detectors were not considered. There are three types of noise in the signal obtained by the framing camera: shot noise, dark current noise and readout noise. Among them, shot noise is the dominating factor to determine the signal-to-noise ratio (SNR). Therefore, we only consider the influence of the shot noise on the precision of the lifetime estimations. To quantify the performance of a lifetime determination scheme, we use the figure of merit introduced by Draaijer *et al.* [25] for the lifetime estimations. The definition is

$$F_\tau(\tau) = \sqrt{N_{tot}} \frac{\sigma_\tau}{\tau}, \tag{8}$$

σ_τ is the standard deviation of τ, and hence σ_τ/τ is the relative standard deviation. And, the figure of merit F_A can also be defined for A,

$$F_A(A) = \sqrt{N_{tot}} \frac{\sigma_A}{A}, \tag{9}$$

where σ_A is the standard deviation of A and σ_A/A is the relative standard deviation. Under a fixed F_i, ($i = \tau, A$), increasing N_{tot} will improve the SNR of τ and A images. If N_{tot} is fixed, an FTI method with a larger F_i, ($i = \tau, A$) has worse precision (larger relative standard deviation).
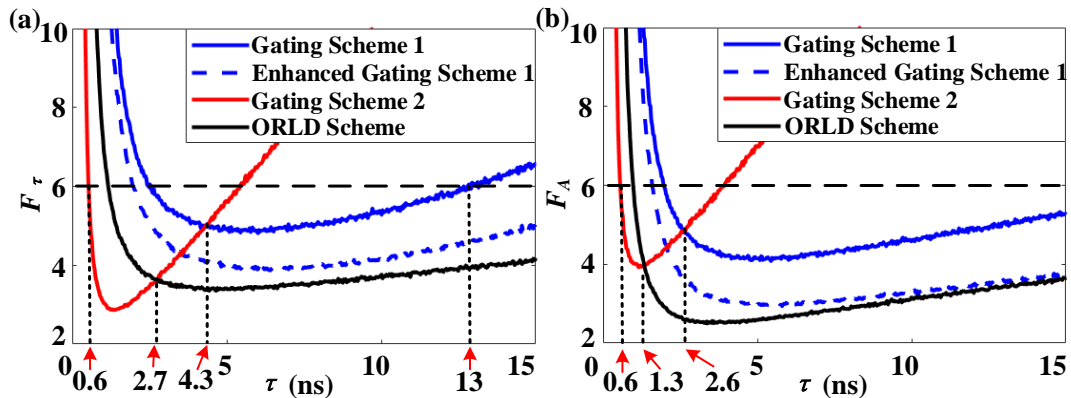
Fig. 4. (a) F_τ and (b) F_A curves as a function of τ for Gating Scheme 1 (blue line), Gating Scheme 2 (red line), enhanced Gating Scheme 2 (dash blue line) and an ORLD scheme ($\Delta t = 2$ns, $Y = 0$, $P = 200$, black line).

Figures 4(a) and 4(b) show the F_τ and F_A curves for Gating Schemes 1 (blue line), 2 (red line), enhanced Gating Scheme 1 (dash blue line) and an ORLD scheme ($\Delta t = 2$ns, $Y = 0$, $P = 200$, black line). For ORLD, two images are captured in a single shot by using two ICCD cameras positioned in a right-angle configuration with a 70/30 beam splitter splitting the signal into two cameras as the DIME works [21]. TFI-TGFLI and OLRD optimize in different lifetime ranges. For TFI-TGFLI, as the number of images acquired in a single-shot increases, the signal intensity of each image decreases, making the F_τ and F_A curves of Gating Scheme 1 larger than ORLD. From the literature [22], the mole fraction of oxygen could vary between 1.64 and 8.36 mol/m^3, the lifetime can vary between 0.7 and 3.0ns. It would be very useful for a FLI instrument to be able to resolve lifetimes in this range. TFI-TGFLI optimizes in the ranges, $\tau < 2.7$ns for F_τ and $\tau < 1.3$ns for F_A, whereas ORLD optimizes in a longer range. ORLD can be adjusted to provide better sensitivity in a certain narrow range [20], whereas TFI-TGFLI can provide a more robust analysis if the lifetime varies significantly within the field of view.

The above simulation results show that we can simply take either τ_1 or τ_2 (similarly A_1 or A_2) images according to the following equations,

$$\tau(x,z) = \begin{cases} \tau_2(x,z), & \tau_2(x,z) < 4.3ns \\ \tau_1(x,z), & else \end{cases}, \tag{10}$$

$$A(x,z) = \begin{cases} A_2(x,z), & \tau(x,z) < 2.6ns \\ A_1(x,z), & else \end{cases}. \tag{11}$$

With Eqs. (10) and (11), we can obtain τ and A images with F_i ($i = \tau$, A) < 6 for $0.6 < \tau < 13$ns and with high precision for $0.6 < \tau < 2.7$ns.

Although Channel 4 was not used in this work, it can be employed to enhance the photon efficiency in the future. If we set the time-gate of Channel 4 the same with that of Channel 1 and merge the two images (Channels 1 & 4), the precision of Gating

Scheme 1 would be further improved. The F_τ and F_A curves (dash blue lines) for the enhanced Gating Scheme 1 is shown in Figs. 4(a) and 4(b). The other advantage of using multi-framing cameras is that we can expand our applications for bi-exponential analysis in the future.

The fluorescence lifetimes of a complex flow may vary significantly according to the temperature, pressure, or quencher concentration gradients. The proposed TFI-TGFLI can achieve single-shot acquisition, provide a wide dynamic range and improve the precision significantly in the short lifetime range, promising wider applications.

4. Analysis of the experimental results

The toluene seeded flows are consisted of N_2 and O_2 with different mixing ratios. Two cases are demonstrated here; Case 1: $N_2:O_2 > 7:0.1$ ($N_2 = 7L/min$; $O_2 < 0.1L/min$. The minimum significant digit that the flow meter can provide is 0.1L/min, therefore any rate lower than this value would indicate 0.0L/min. Thus, we tuned the meter of the O_2 supply for Case 1 to 0.0L/min, but the actual flow rate should be $< 0.1L/min$) and Case 2: $N_2:O_2 = 19:1$ ($N_2 = 19L/min$; $O_2 = 1L/min$). From the fluorescence lifetimes we obtained in the experiments described below, we could conclude that the $N_2:O_2$ ratio for Case 1 could be up to 120:1 whereas the measured lifetime $\tau = 2.6ns$ for Case 2 is in a good agreement with the literature compared with the results reported in [22, 26]. The purpose of the experiments designed for this work is to evaluate the performances of the proposed lifetime determination methods, and the experiments indeed confirm that the measurements obtained from the proposed camera are in good agreement with those obtained by the streak camera.

The three normalized fluorescent intensity images captured by the framing camera for Case 1, are shown in Figs. 5 (a)-5(c). Figures 5(d)-5(f) are the three intensity images for Case 2. All the intensity images have the same size of 200×170 pixels. For Case 1, the signal-to-noise (SNR) ratios of Figs. 5(a)-5(c) are 11.78, 12.74, and 10.33dB, respectively. For Case 2, the SNRs of Figs. 5(d)-5(f) are 8.67, 8.96, and 8.39dB, respectively.
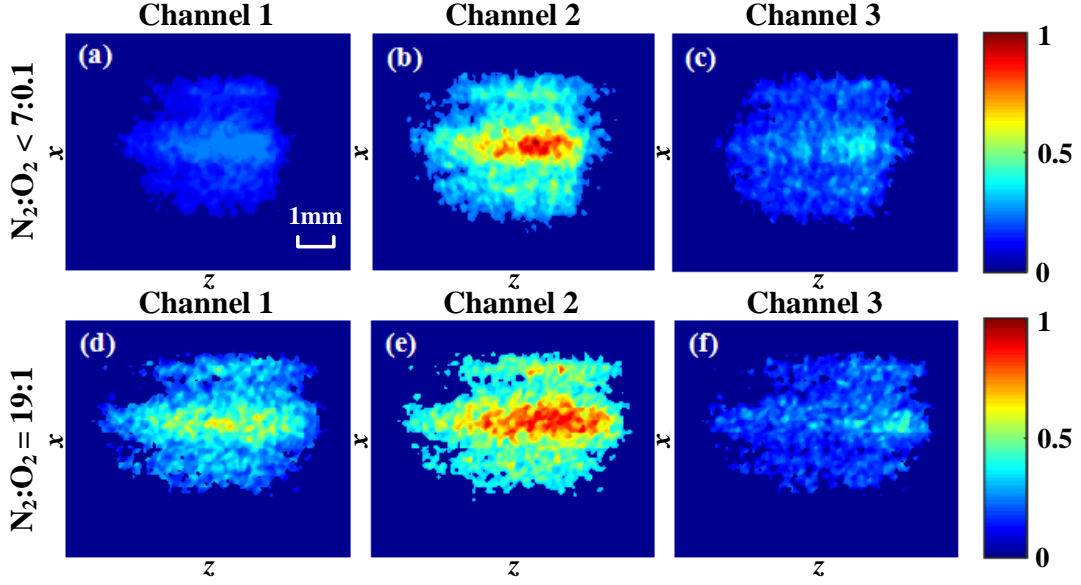
Fig. 5. Normalized fluorescent intensity images captured by the three channels of the framing camera for Case 1 (N$_2$:O$_2$ > 7:0.1), (a), (b), and (c), and Case 2 (N$_2$:O$_2$ = 19:1), (d), (e), and (f).

τ and A images can be calculated from the three intensity images shown in Fig. 5 using the lifetime determination algorithm mentioned in Section 3. In order to visualize the distributions of the toluene molecules, the intensity profile of the pulsed laser I_v should be confirmed. We assume that the intensity of the laser approximately stays the same along the propagation (+z) axis through the target flow and has a Gaussian distribution perpendicular to the propagation direction (+x), i.e.

$$I_v(x) = I_0 \exp\left\{-\left[2\sqrt{2}\left(x - x_0\right)/x_v\right]^2\right\},$$ where I_0 is the peak intensity, x_0 is the position

of the peak value, and x_v is the full width at half maximum (FWHM). Then the relative concentration distributions n_1^0 can be obtained from Eq. (4).

Figs. 6(a) and 6(b) show the lifetime and the normalized n_1^0 images for Case 1 (N$_2$:O$_2$ > 7:0.1), whereas Figs. 6(c) and 6(d) show the lifetime and n_1^0 images for Case 2 (N$_2$:O$_2$ = 19:1). Fig. 6(e) shows the sectional view of the gas jet. The red dotted box indicates the gas jet section illuminated by the laser sheet. The two lifetime images in Figs. 6(a) and 6(c) are uniform, implying that the distributions of the quencher (O$_2$ and N$_2$) concentrations are uniform. The two normalized n_1^0 images shown in Figs. 6(b) and

6(d) indicate that the fluorophore (toluene) concentration distributions are rich in the central area, but poor at the edges along the z axis. The effects that the uneven distributions along the x axis could be caused by the actually non-Gaussian distributed laser sheet. The observations from Fig. 6 are in line with the experimental settings, shown in Fig. 6(e), having the gas flows with relatively uniform distributions in temperature, pressure, and quencher concentrations, but with more toluene molecules distributed in the area above the jet tube and less around the edges (the reason is likely due to gas diffusion).
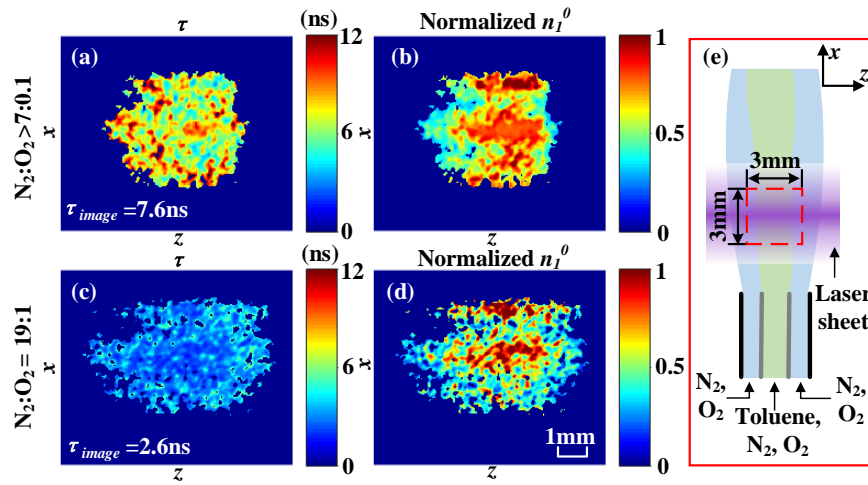

Fig. 6. Fluorescence lifetime images for (a) $N_2:O_2 > 7:0.1$ and for (c) $N_2:O_2 = 19:1$, and n_1^0 images for (b) $N_2:O_2 > 7:0.1$ and for (d) $N_2:O_2 = 19:1$. (e) Sectional view of the gas jet.

The variable, τ_{image}, in Figs. 6(a) and 6(c) means the average lifetime for the whole excited area. Figures. 7(a) and 7(b) show τ_{image} for ten repeated experiments for Cases 1 and 2, respectively. For Case 1, τ_{image} is calculated by using Gating Scheme 1, the average τ_{image} is $\tau_{mean} = 7.7$ns and the standard deviation among these experiments is $\sigma_\tau^{mean} = 200$ps as shown in Fig. 7(a). For Case 2, τ_{image} is calculated by using Gating Scheme 2, $\tau_{mean} = 2.6$ns and $\sigma_\tau^{mean} = 80$ps (but when we used Gating Scheme 1 for this, we obtained $\sigma_\tau^{mean} = 150$ps). It is convincing that the accuracy of the lifetime measurements is improved in the short lifetime range using TFI-TGFLI rather than using only one ORLD scheme (Gating Scheme 1) to measure both long and short

lifetimes. To use ORLD properly, it is necessary to have better understanding about the lifetime distribution beforehand. The scatter plots, τ in the estimated lifetime images Figs. 6(a) and 6(c) vs the intensity in the corresponding intensity images Figs. 5(b) and 5(e), and the lifetime histograms for Experiment 1 are shown in Figs. 7(c) and 7(d), respectively. For Case 1 (blue), $\tau_{image} = 7.6$ns and the standard deviation for all the pixels in the lifetime image is $\sigma_\tau^{image} = 1.7$ns. For Case 2 (red), $\tau_{image} = 2.6$ns and $\sigma_\tau^{image} = 0.8$ns. As the gain of the ICCDs used in Case 1 is bigger than that used in Case 2, the largest intensity in Case 1 is larger than that in Case 2. The scatter plot for Case 1 contains 123 saturated pixels (peaked at 2^{14}-1), and they are contributed by the saturated 14-bit A/D converter. The statistical results are, however, not influenced. We can tune the gain in the future to avoid saturated pixels.
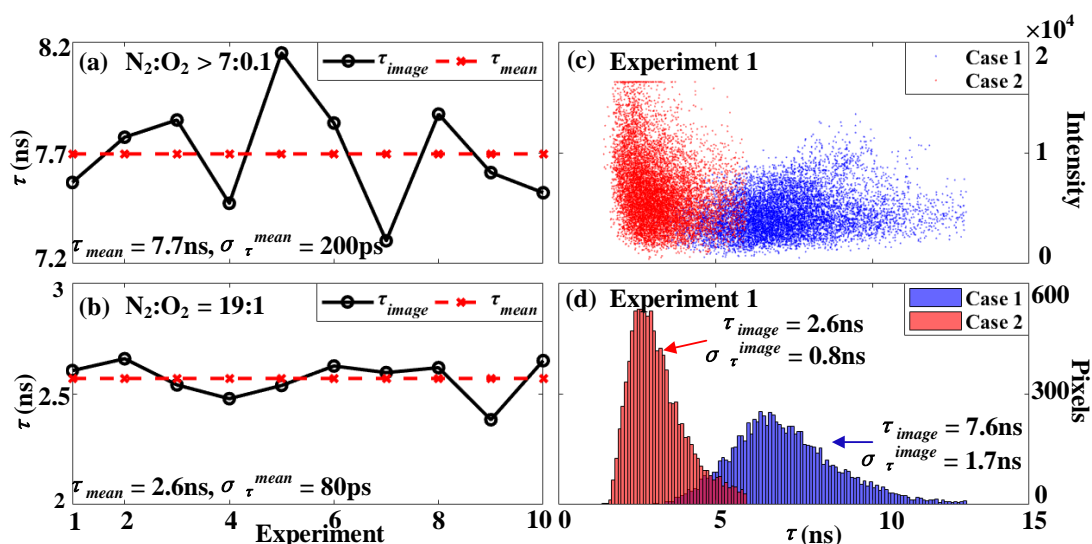

Fig. 7. Lifetime curves for (a) $N_2:O_2 > 7:0.1$ and for (b) $N_2:O_2 = 19:1$ among ten repeated experiments. (c) Scatter plots and (d) lifetime histograms for Case 1 (blue) and Case 2 (red) for Experiment 1.

Next, we compared the results obtained by the proposed method with those obtained from a streak camera. Fig. 8(a) is the background image before the sweep voltage of the streak camera is turned on, and Figs. 8(b) and 8(c) are the normalized intensity images recorded by the streak camera for Case 1 ($N_2:O_2 > 7:0.1$) and Case 2

(N_2:O_2 = 19:1), respectively. The A/D converter of the ICCD in the streak camera is 16-bit, and the actual peak intensities for Figs. 8(b) and 8(c) are 5400 and 2000, respectively. By integrating the images in Figs. 8(b) and 8(c) over the x axis, we obtained 1D normalized intensity curves (red lines) for Cases 1 and 2, as shown in Figs. 8(e) and 8(f). The blue open circle lines represent the results of TFI-TGFLI. Figs. 8(g) and 8(h) show the semi-log intensity curves for Cases 1 and 2. As the direction of the gas jet is parallel to the slit of the streak camera, the width of the slit is wide and a UV lens was used to gather the signal to the streak camera, the fluorescence from the total excitation region was collected by the streak camera. The temporal resolution is, however, deteriorated such that the signal detected in each scanning step has a duration of 5ns, as shown in Fig. 8(a). The images obtained by the streak camera are the signal decay functions convolved with the instrumental function that is caused by the slit, i.e., the signals from the adjacent scanning steps (200ps interval) have an overlap, as shown in Fig. 8(d). $S_1 \sim S_n$ represent n scanning steps, with the shadowed areas representing the overlaps. After performing the convolution process, the results obtained by TFI-TGFLI agreed well with the results obtained from the streak camera, as shown in Figs. 8(e)-8(h). We can conclude that the estimated average lifetimes are credible. Note that the tails (< 1/10 peak values) were not fitted well due to the noise. If the integral time of the streak camera increases, the fitting results would be better.
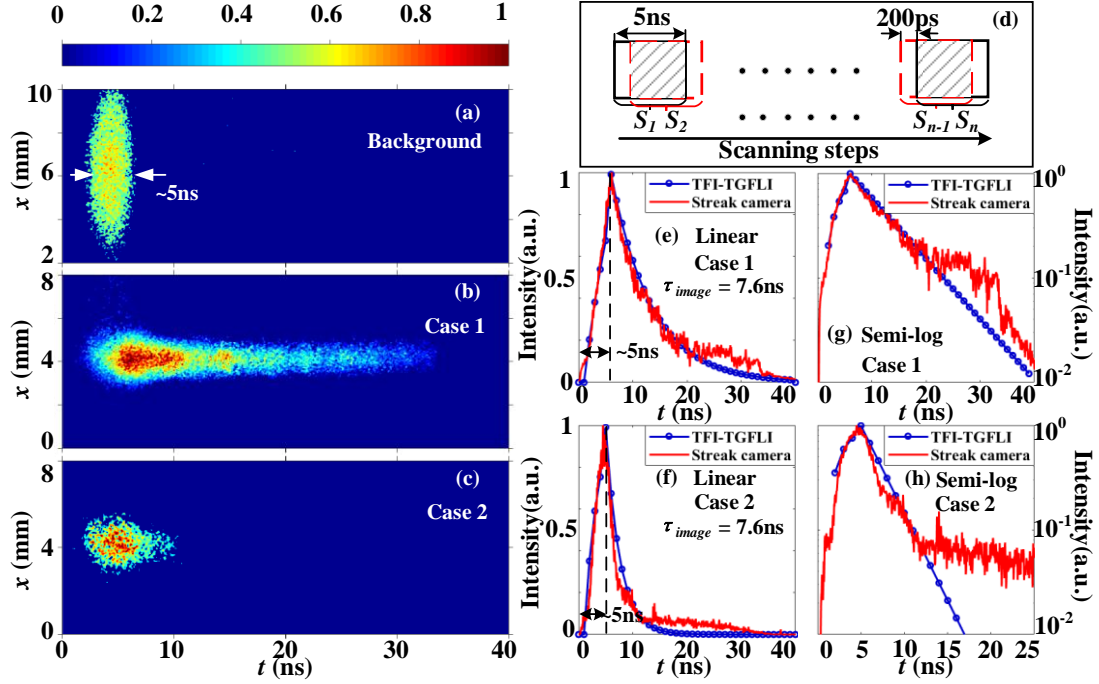
Fig. 8. (a) Background image without scanning, and the 1D lifetime images for (b) Case 1 and (c) Case 2 captured by the streak camera. (d) Schematic diagram representing the scanning of the streak camera. Linear intensity curves for (e) Case 1 and (f) Case 2 obtained by integrating the 1D lifetime images (b) and (c) over the x axis (red solid lines). The blue open circle lines represent the calculated results obtained by TFI-TGFLI. Semi-log intensity curves for (g) Case 1 and (h) Case 2.

5. Conclusion

We proposed a new rapid lifetime determination scheme on a multi-channel framing camera to achieve single-shot fluorescence lifetime imaging based on three images, and we coined it as TFI-TGFLI. The method combines the advantages of PLIF, time-gated FLI, and a multi-channel framing camera to perform single-shot acquisition. The proposed TFI-TGFLI has a wide lifetime measurement range, 0.6 ~ 13ns, under the figure of merit $F_i < 6$, ($i = \tau, A$). The lifetime images of the toluene seeded in gas mixtures of nitrogen and oxygen with different ratios were measured. Under $N_2:O_2 > 7:0.1$ ($N_2 = 7$L/min; $O_2 < 0.1$L/min) and $N_2:O_2 = 19:1$ ($N_2 = 19$L/min; $O_2 = 1$L/min) conditions, the measured average lifetimes of the whole excited areas are 7.6ns and 2.6ns with the standard deviations of 1.7ns and 0.8ns among the lifetime image pixels ,

respectively. They are consistent with the results obtained by the streak camera. A further analysis on the relative concentrations of the quenchers and the fluorescent species shows a good agreement with the experimental settings. We believe that TFI-TGFLI can be an effective tool for complex flow diagnosis.

References

1. S. D. Hammack, C. D. Carter, J. R. Gord, and T. Lee, "Nitric-oxide planar laser-induced fluorescence at 10 kHz in a seeded flow, a plasma discharge, and a flame," Appl. Opt. **51**(36), 8817–8824 (2012).

2. M. P. Lee, P. H. Paul, and R. K. Hanson, "Quantitative imaging of temperature fields in air using planar laser-induced fluorescence of O_2," Opt. Lett. **12**(2), 75–77 (1987).

3. Z. K. Wang, P. Stamatoglou, Z. M. Li, M. Alden, and M. Richter "Ultra-high-speed PLIF imaging for simultaneous visualization of multiple species in turbulent flames," Opt. Express **25**(24), 30214–30228 (2017).

4. A. Ehn, J. J. Zhu, X. S. Li, and J. Kiefer, "Advanced laser-based techniques for gas-phase diagnostics in combustion and aerospace engineering," Appl. Spectrosc. **71**(5), 1–26 (2017).

5. C. Brackmann, J. Bood, J. D. Naucler, A. A. Konnov, and M. Alden, "Quantitative picosecond laser-induced fluorescence measurements of nitric oxide in flames," Proc. Combust. Inst. **36**, 4541–4548 (2016).

6. B. Zhou, C. Brackmann, Q. Li, Z. K. Wang, P. Petersson, Z. S. Li, M. Ald´en, and X. S. Bai, "Distributed reactions in highly turbulent premixed methane/air flames. Part I. Flame structure characterization," Combust. Flame **162**, 2937–2953 (2015).

7. J. Philip, and K. Carlsson, "Theoretical investigation of the signal-to noise ratio in fluorescence lifetime imaging," J. Opt. Soc. Am. A **20**(2), 368–379 (2003).

8. H. C. Gerritsen, A. V. Agronskaia, A. N. Bader, and A. Esposito, "Time domain FLIM: Theory, instrumentation, and data analysis" in Laboratory Techniques in Biochemistry and Molecular Biology, T. W. J. Gadella, ed. (Elsevier, 2009), pp. 95–132.

9. W. Becker, *Advanced Time-Correlated Single Photon Counting Techniques*,

(Springer, 2005).

10. G. O. Fruhwirth, S. A. Beg, R. Cook, T. Watson, T. Ng, and F. Festy, "Fluorescence lifetime endoscopy using TCSPC for the measurement of FRET in live cells," Opt. Express **18**(11), 11148–11158 (2010).

11. S. Isbaner, N. Karedla, D. Ruhlandt, S. C. Stein, A. Chizhik, I. Gregor, and J. Enderlein, "Dead-time correction of fluorescence lifetime measurements and fluorescence lifetime imaging," Opt. Express **24**(9), 9429–9445 (2016).

12. J. McGinty, J. R. Isidro, I. Munro, C. B. Talbot, P. A. Kellett, J. D. Hares, C. Dunsby, M. A. A. Neil, and P. M. W. French, "Signal-to-noise characterization of time-gated intensifiers used for wide-field time-domain FLIM," J. Phys. D: Appl. Phys. **42**, 135103 (2009).

13. X. F. Wang, T. Uchida, D. M. Coleman, and S. Minami, "A two-dimensional fluorescence lifetime imaging system using a gated image intensifier," Appl. Spectrosc. **45**(3), 360–366 (1991).

14. D. D. U. Li, S. Ameer-Beg, J. Arlt, D. Tyndall, R. Walker, D. R. Matthews, V. Visitkul, J. Richardson, and R. K. Henderson, "Time-domain fluorescence lifetime imaging techniques suitable for solid-state imaging sensor arrays," Sensors **12**(5), 5650-5669 (2012).

15. E. Gratton, M. Limkeman, J. R. Lakowicz, B. P. Maliwal, H. Cherek, and G. Laczko, "Resolution of mixtures of fluorophores using variable-frequency phase and modulation data," Biophys. J. **46**, 479-486 (1984).

16. M. A. Digman, V. R. Caiolfa, M. Zamai, and E. Gratton, "The phasor approach to fluorescence lifetime imaging analysis," Biophys. J. **94**, L14-L16 (2008).

17. M. Jonsson, A. Ehn, M. Christensen, M. Alden, and J. Bood, "Simultaneous one-dimensional fluorescence lifetime measurements of OH and CO in premixed flames," Appl. Phys. B Lasers Opt. **115**, 35–43 (2014).

18. A. Omrane, F. Ossler, and M. Aldén, "Two-dimensional surface temperature measurements of burning materials," Proc. Combust. Inst. **29**(2), 2653-2659 (2002).

19. A. Ehn, O. Johansson, J. Bood, A. Arvidsson, B. Li, and M. Alden, "Fluorescence lifetime imaging in a flame," Proc. Combust. Inst. **33**(1), 807–813 (2011).

20. S. P. Chan, Z. J. fuller, J. N. Demas, and B. A. DeGraff, "Optimized gating scheme for rapid lifetime imaging," Anal. Chem. **73**(18), 4486–4490 (2001).

21. A. Ehn, O. Johansson, A. Arvidsson, M. Alden, and J. Bood, "Single-laser shot fluorescence lifetime imaging on the nanosecond timescale using a Daul Image and Modeling Evaluation algorithm," Opt. Express **20**(3), 3044–3056 (2012).

22. A. Ehn, M. Jonsson, O. Johansson, M. Alden, and J. Bood, "Quantitative oxygen concentration imaging in toluene atmospheres using Dual Imaging with Modeling Evaluation," Exp. Fluids **54**, 1433 (2013).

23. R. K. Hanson, R. M. Spearrin, and C. S. Goldenstein, *Spectroscopy and Optical Diagnostics for Gases*, (Springer, 2016), Chap. 11.

24. D. U. Li, E. Bonnist, D. Renshaw, and R. Henderson, "On-chip, time-correlated, fluorescence lifetime extraction algorithms and error analysis," J. Opt. Soc. A **25**(5), 1190–1198 (2008).

25. A. Draaijer, R. Sanders, and H. C. Gerritsen, "Fluorescence lifetime imaging, a new tool in confocal microscopy," in *Handbook of Biological Confocal Microscopy*, J. B. Pawley, ed. (Plenum, 1995), pp. 491–505.

26. S. Faust, T. Dreier, and C. Schulz, "Temperature and bath gas composition dependence of effective fluorescence lifetimes of toluene excited at 266 nm," Chem. Phys. **383**, 6–11 (2011).